Geomech. Geophys. Geo-energ. Geo-resour. (2024) 10:100
https://doi.org/10.1007/s40948-024-00825-2

RESEARCH

Characteristics of waterproof failure and optimal width of narrow coal pillars under the coupled effects of mining, excavation and seepage

Dingchao Chen · Xiangyu Wang · Jianbiao Bai · Menglong Li

Received: 18 December 2023 / Accepted: 27 May 2024

Abstract The failure of waterproof coal pillars under the coupled effects of mining, excavation and water seepage is a significant factor contributing to sudden water inflow accidents in underground roadways. Investigating the instability characteristics and optimal width of waterproof coal pillars holds vital significance for water control and resource protection in mines. This study focus on the rational width of waterproof coal pillar at Dongzhuang Coal Mine in Shanxi Province. Using FLAC^{3D}, a fluid–structure interaction numerical model of waterproof coal pillar was established, revealing the coupling characteristics of stress fields, plastic zones, and seepage zones within coal pillars under the influence of mining, excavation and water infiltration weakening. Furthermore, the stability characteristics of waterproof coal pillars with different widths were compared. The results are as follows: (1) Under the combined action of overlying strata pressure and water pressure from the gob, the coal mass on the water-inflow side of coal pillar is the first to fail. Additionally, with the infiltration of water, the elastic modulus, cohesion, and friction angle of the coal mass in the seepage zone decrease. (2) The lifecycle of waterproof coal pillar can be divided into three stages: working face mining, water infiltration from the gob, and roadway excavation. Based on this, the connectivity between plastic zones and seepage zones serves as the critical condition for the stability of waterproof coal pillar was proposed. (3) When the width of waterproof coal pillar is 3 m and 5 m, plastic zones become connected, forming a water-conducting channel. When the width of waterproof coal pillar is 7 m, 9 m, and 11 m, seepage zones and plastic zones are not connected, and the coal pillar exhibits load-bearing and water-barrier properties.

D. Chen · X. Wang (✉) · J. Bai · M. Li
Key Laboratory of Deep Coal Resource Mining, China University of Mining and Technology, Xuzhou 221116, China
e-mail: wangxiangyu79@126.com

D. Chen · X. Wang · M. Li
School of Mines, China University of Mining and Technology, Xuzhou 221116, China

J. Bai
State Key Laboratory of Coal Resources and Safe Mining, China University of Mining and Technology, Xuzhou 221116, China

Highlights

(1) A numerical model for fluid–structure interaction of waterproof coal pillar along the gob-side roadway was established.
(2) A Fish language program was developed to account for the weakening of waterproof coal pillar due to water immersion.
(3) The coupling characteristics of stress distribution, plastic zones, and seepage zones of waterproof coal pillar during “mining—water immer-

Published online: 05 June 2024

sion softening—roadway excavation" stages were revealed.

Keywords Waterproof coal pillar · Fluid–structure interaction · Water immersion softening · Damage degree · Permeability

1 Introduction

During the underground coal mining process, there are various hazards, among which water inrush accidents rank as the second most significant disaster, following closely behind gas-related incidents (Ma and Bai 2015; Dash et al. 2016; Sun et al. 2016; Wang et al. 2022a). According to statistics from 2001 to 2022, there have been 1105 water inrush accidents in Chinese coal mines, resulting in a total of 4491 fatalities (Fangpeng et al. 2018; Yin et al. 2023) (Fig. 1).

The presence of water inrush accidents poses a tremendous threat to the safety of coal mining operations (Maiti et al. 2009; Bukowski 2015; Ma et al. 2019; Wang et al. 2022b; Liu et al. 2023a). During the excavation of roadways, various water inrush problems are frequently encountered (Gui and Lin 2016; Polak et al. 2016). When a water inrush occurs, groundwater rapidly flows into roadway through fractures in rock mass under the influence of water pressure (Ma et al. 2022; Liu et al. 2023b). Failure to promptly discharge the inflowing water can lead to the flooding of roadway, resulting in the scrapping of mining equipment at best and causing severe injuries or fatalities to personnel at worst (Singh 2015; Zhao et al. 2020). The influx of large amounts of groundwater into roadway also weakens the surrounding rock properties, significantly reducing the overall stability of roadway and leading to disasters such as roof collapse and floor heave (Cui et al. 2018; Ma et al. 2018). Furthermore, the ingress of groundwater can cause irreversible damage to roadway, making repairs extremely difficult and costly, and sometimes even rendering roadway irreparable (Zhang et al. 2019b).

To prevent water inrush disasters, it is common practice in mine development to leave a certain width of coal pillars between adjacent working faces, as shown in Fig. 2, to block the accumulation of water in the gob (Wang et al. 2021; Chen et al. 2022a; Galav et al. 2022; He and Huang 2022; Fang et al. 2023). The stability of these waterproof coal pillars has long been one of the critical research topics in coal mine development (Wang 2006; Hu et al. 2019; Li et al. 2021; He et al. 2023).

Experimental research is an important method for studying waterproof coal pillars (Chen et al. 2022b). Currently, experimental investigations on waterproof coal pillars primarily focus on the weakening effects of water content on the mechanical parameters of coal samples (Yao et al. 2021b). Yao et al. (2020) conducted tests involving variable-angle shear on coal samples with different water contents, while (Lu et al. 2016; Wang et al. 2018; Zhang and Nie 2020) performed uniaxial and triaxial tests on coal samples with varying water contents. The findings from these

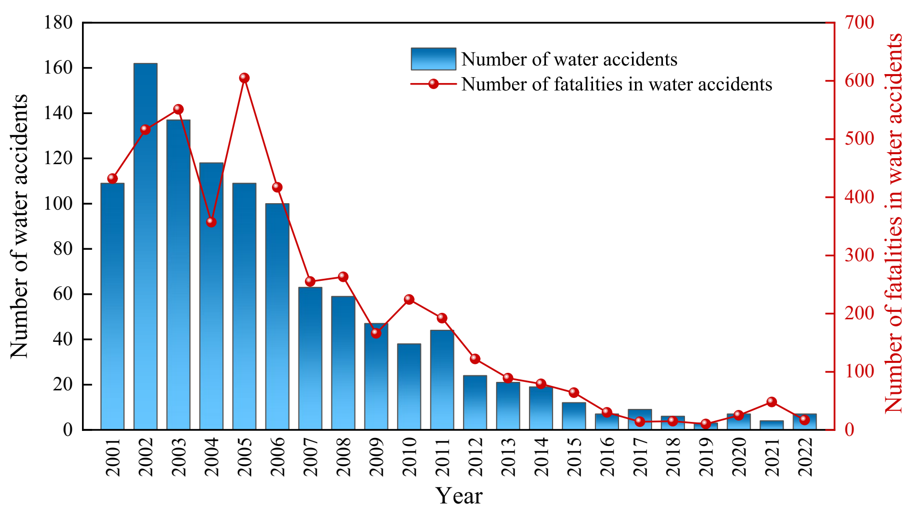

Fig. 1 Statistics of water inrush accidents in Chinese coal mines during 2001–2022

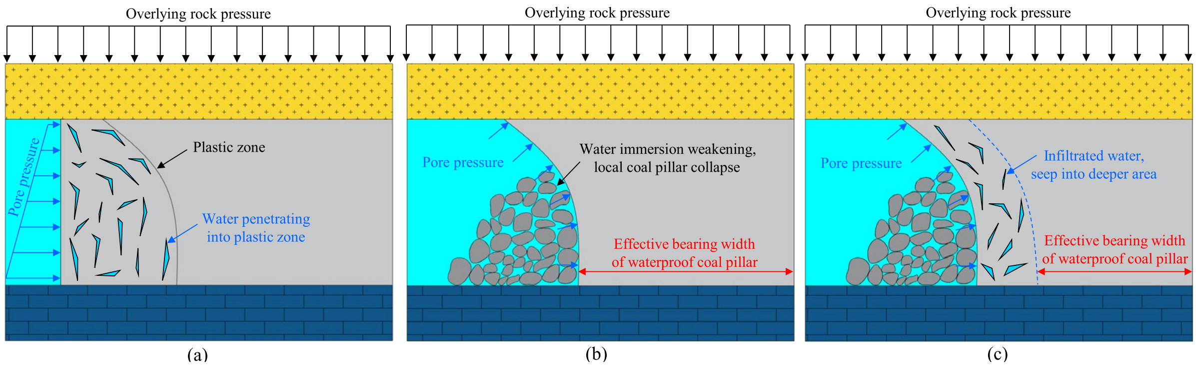

Fig. 2 Illustration of the water immersion failure process of waterproof coal pillar: **a** seepage of water from the gob into the plastic zone of waterproof coal pillar; **b** weakening and collapse of coal pillar's plastic zone due to water immersion; **c** seepage of water from the gob into the deeper region of waterproof coal pillar

studies consistently demonstrate that the mechanical properties of coal pillars, such as compressive strength, shear strength, friction angle, and cohesion, decrease with an increase in water content.

Furthermore, numerical simulations play a crucial role in studying waterproof coal pillars. Liu et al. (2020) analyzed the effects of coal pillar width, dip angle, and water pressure on the stability of waterproof coal pillars. Their findings suggest that water pressure has a more significant influence than coal seam dip angle, which, in turn, has a more significant impact than coal pillar width when the coal pillar width ranges from 12 to 18 m, water pressure varies from 0 to 0.3 MPa, and coal seam dip angle ranges from 2° to 10°. Shao et al. (2022) simulated waterproof coal pillars under fault conditions, examining damage and water inrush situations. Additionally, Chen et al. (2017) simulated the evolution of internal fractures within waterproof coal pillars.

Scholars have made substantial contributions in experimental and simulation research regarding waterproof coal pillars (Zhang et al. 2023). However, in existing studies, experimental research has been unable to fully reveal the actual situation of waterproof coal pillars, and simulation studies have not highlighted the complete cycle of failure mechanisms for waterproof coal pillars. The Dongzhuang Coal Mine has decided to advance the 30,204 tailgate along the water-containing gob side in order to improve the coal recovery rate. During this process, the coal pillar in the section will undergo the mining effects of the 30,203 panel, water infiltration in the gob, and disturbances caused by the excavation of the 30,204 tailgate. In light of this, this study employs FLAC^{3D} to establish a fluid–structure interaction model for waterproof coal pillars, developing a system to assess the weakening of coal pillars due to water inflow during roadway excavation. By employing real-time monitoring of zone's elastic–plastic state, stress, strain, and water saturation, the dynamic updating of mechanical parameters within coal pillar is achieved. This approach has uncovered the instability mechanism of waterproof coal pillars during "mining—water immersion softening—roadway excavation" coupling effect while driving roadway along gob. The result of this research is of significant importance for determining the width and stability analysis of waterproof coal pillars.

2 Development of fluid–structure interaction system

2.1 Calculation of coal pillar permeability

After the mining of working face, segmented coal pillar undergo prolonged stress variation and damage, leading to varying degrees of internal structural changes and alterations in physical properties. Consequently, it is necessary to separate internal zones of coal pillar into elastic and plastic zones for individual calculations. In this study, the permeability of waterproof coal pillar is calculated using the permeability formula proposed by (Zhang et al. 2019a):

$$k_E = 7.9549e^{-4.8879\left(1-e^{-0.3888\sigma_1}\right)} \tag{1}$$

$$k_P = 142.2316e^{-2.6349\left(1-e^{-0.3415\sigma_1}\right)} \tag{2}$$

where, k_E is the permeability of coal samples in elastic state, md; k_P is the permeability of coal samples in plastic state, md; σ_1 is effective stress, MPa.

The relationship between the permeability of coal samples and effective stress is illustrated in Fig. 3. The permeability of coal samples is significantly higher in plastic state than in elastic state. Distinguishing between elastic and plastic states is crucial for fluid–structure interaction calculation of coal, as it can significantly improve the accuracy of the prediction results.

2.2 Coal pillar weakening criterion

Existing research suggests that water gradually infiltrates into coal pillars, and when water pressure gradient exceeds initiation pressure gradient of coal pillars, permeation occurs (Yao et al. 2022). The relationship between initiation pressure gradient of coal pillars and permeability follows a power-law function, as shown below:

$$G = 0.03252k^{-1.4155} \tag{3}$$

where G is initiation pressure gradient of coal pillars, MPa/cm; k is permeability, m^2.

When coal pillars are subjected to water infiltration, their mechanical properties are weakened. Based on numerous laboratory experiments, Xue (2017), Yao et al. (2021a) have identified that elastic modulus, cohesion, and friction angle of coal exhibit negative exponential relationships with water saturation. The softening coefficients due to water infiltration are given by:

$$\begin{cases} l_E = 0.8947e^{\left(-S_w/68.36\right)} + 0.1053 \\ l_C = 0.31496e^{\left(-S_w/37.36\right)} + 0.685 \\ l_\varphi = 0.0638e^{\left(-S_w/2.08\right)} + 0.9362 \end{cases} \tag{4}$$

where l_E is the weakening coefficient of elastic modulus; l_C is the weakening coefficient of cohesion; l_φ is the weakening coefficient of friction angle; S_w is water saturation, % (Fig. 4).

2.3 Calculation of coal pillar damage

In the process of mining, coal pillars are influenced by mining, water immersion and excavation, leading to plastic deformation of coal pillars (Zhang et al. 2021). Previous studies mostly focused on monitoring a single cross-section to observe the characteristics of plastic zone. However, in reality, coal pillars are three-dimensional structures, and observing only one cross-section is insufficient to describe

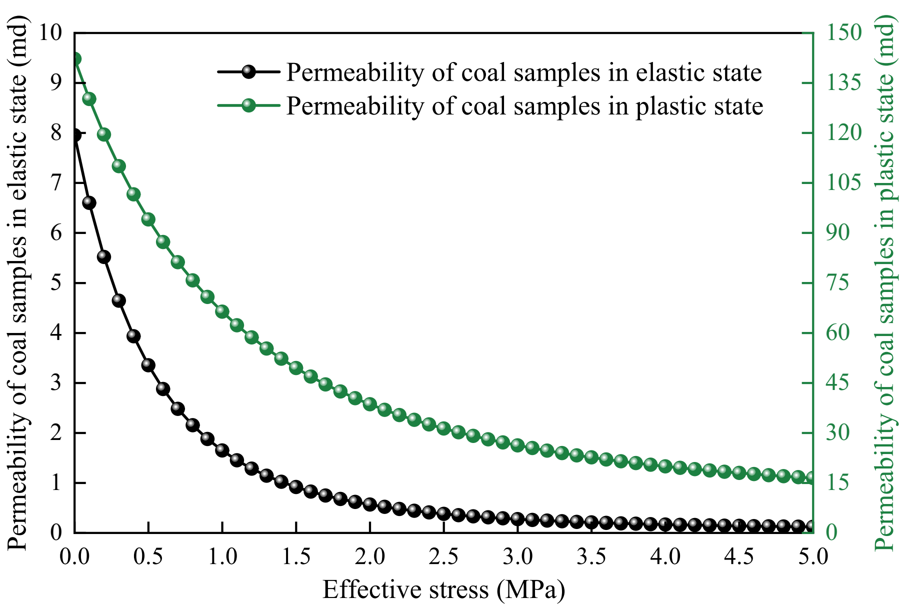

Fig. 3 The relationship between the permeability of coal samples and effective stress

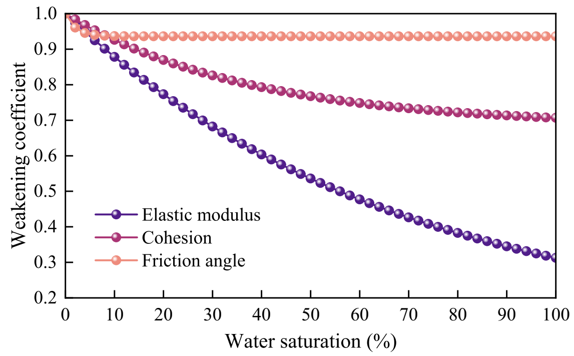

Fig. 4 The relationship between the weakening coefficient and water saturation

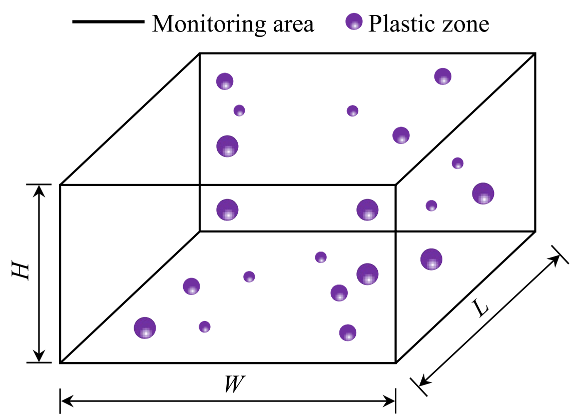

Fig. 5 Calculation model for coal pillar damage degree

the overall plastic behavior of pillars (Han et al. 2022). Therefore, this study introduces the concept of "coal pillar damage degree," defined as the ratio of the total volume of plastic zones in monitoring area to the volume of the entire monitoring area, as shown in Fig. 5.

$$D = \frac{\sum_{i=1}^{n} V_i}{V} \times 100\% \tag{5}$$

where, D is coal pillar damage degree; V_i is the volume of a plastic zone; V is the volume of monitoring area.

$$V = LWH \tag{6}$$

where L is the length of monitoring area, m; W is the width of coal pillar, m; H is the height of coal pillar, m.

2.4 Overview of deviatoric stress indicators

Based on the theory of elastoplastic mechanics (Wang et al. 2022c), the stress tensor can be divided into deviatoric stress tensor (the first term on the right of Eq. 7) and spherical stress tensor (the second term on the right of Eq. 7). The deformation of an object is primarily caused by changes in volume and shape, where the deviatoric stress tensor induces changes in the shape of the object, and the spherical stress tensor induces changes in the volume of the object (Shan et al. 2021).

$$\begin{bmatrix} \sigma_1 & 0 & 0 \\ 0 & \sigma_2 & 0 \\ 0 & 0 & \sigma_3 \end{bmatrix} = \begin{bmatrix} \sigma_1 - \sigma_m & 0 & 0 \\ 0 & \sigma_2 - \sigma_m & 0 \\ 0 & 0 & \sigma_{3-\sigma_m} \end{bmatrix} + \begin{bmatrix} \sigma_m & 0 & 0 \\ 0 & \sigma_m & 0 \\ 0 & 0 & \sigma_m \end{bmatrix} \tag{7}$$

where, σ_1, σ_2 and σ_3 are the principal stresses in three mutually perpendicular directions, MPa; σ_m is the spherical stress tensor, and its expression is as follows:

$$\sigma_m = \frac{\sigma_1 + \sigma_2 + \sigma_3}{3} \tag{8}$$

where, $\sigma_i - \sigma_m$ (i=1,2,3) is the deviatoric stress. In this study, the deformation and failure characteristics of waterproof coal pillar are analyzed based on the maximum deviatoric stress, which can be expressed as follows:

$$\sigma\prime = \sigma_1 - \sigma_m = \sigma_1 - \frac{\sigma_1 + \sigma_2 + \sigma_3}{3} \tag{9}$$

2.5 Operation process of fluid–structure interaction system

Combining Eqs. (1) and (2), the permeability tensor components k_{E1}, k_{E2} and k_{E3} in elastic zone, as well as the permeability tensor components k_{P1}, k_{P2} and k_E in plastic zone can be obtained, as illustrated in Fig. 6. Among these, k_{P1} and k_{P2} lie on the fracture surface and are perpendicular to each other, while k_E is perpendicular to the fracture surface (Li et al. 2023).

Building upon the aforementioned foundation, this study developed a Fish-language program for water-inrush weakening of waterproof coal pillars using FLAC^{3D}. Through iterative calculations, a dynamic coupling between seepage parameters and coal pillar

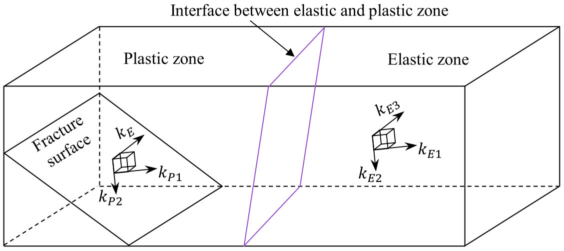

Fig. 6 Permeability tensor of internal zones in coal pillar

mechanical properties is achieved. The specific workflow is illustrated in Fig. 7.

3 Reconstruction of mechanical environment for waterproof coal pillars

3.1 Project overview

The 3# coal at Dongzhuang Coal Mine in Shanxi has a burial depth of approximately 350 m and a thickness of 2.5 m. It is a nearly horizontal coal seam. The 30,203 panel has been fully mininged, resulting in a significant accumulation of water in the gob. The elevation of the 30,204 panel ranges from +720 to

Fig. 7 Operation process of fluid–structure interaction system

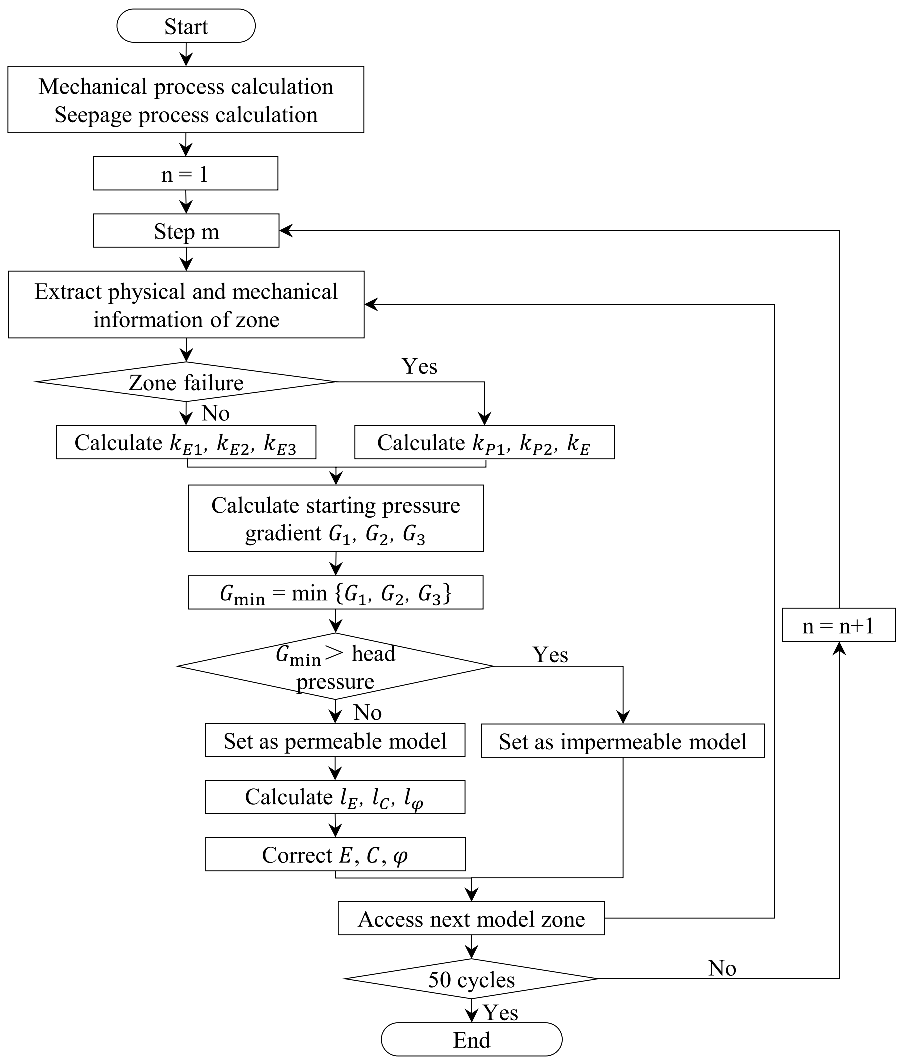

+750 m, with a strike length of 150 m. The 30,204 tailgate is planned to adopt a method of mining small coal pillars along the gob, as illustrated in Fig. 8. The waterproof coal pillar between 30,203 gob and 30,204 panel is influenced by factors such as mining-induced stress, water infiltration weakening, and excavation disturbances. It is necessary to conduct stability studies to ensure safe mining production in the mine.

Based on the geological information provided by Dongzhuang Coal Mine, a borehole profile for 30,204 panel is constructed, as shown in Fig. 9. The strata above 3# coal include a 1.0 m thick mudstone, a 1.8 m thick siltstone, a 5.6 m thick mudstone, and a 2.6 m thick medium sandstone, which are characterized as weak to semi-hard rock layers. Below 3# coal, there is a 4.0 m thick mudstone, also categorized as weak to semi-hard rock layer.

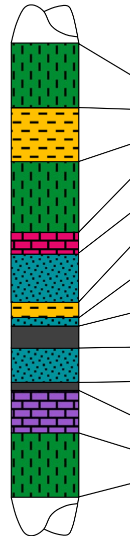

Lithology	Thickness/m	Depth/m
Sandy mudstone	7.0	319.6
Siltstone	6.2	325.8
Sandy mudstone	8.1	333.9
Medium sandstone	2.6	336.5
Mudstone	5.6	342.1
Siltstone	1.8	343.9
Mudstone	1.0	344.9
3# Coal	2.5	347.4
Mudstone	4.0	351.4
Coal	0.9	352.3
Fine sandstone	4.9	357.2
Sandy mudstone	7.4	364.6

Fig. 9 Borehole profile of 30,204 panel

3.2 The establishment of numerical model

Based on the on-site engineering survey, a FLAC^{3D} fluid–structure interaction numerical simulation model is established with dimensions of 180 m × 300 m × 52 m. The roadway size is set as 5.2 m × 3.5 m, with a total of 547,200 elements and 569,618 nodes, as shown in Fig. 10. The simulation progresses through three sequential stages based on the actual mining sequence: "mining of 30,203 panel to form the gob (Stage 1) → water erosion in 30,203 gob, causing infiltration into coal pillar (Stage 2) → excavation of 30,204 tailgate, leading to deformation and failure of coal pillar". The model is constrained at the bottom, simply supported on four sides, and subjected to an 8.0 MPa load on top to simulate the load from overlying strata. In the second stage, a water pressure of 0.1 MPa is applied along the gob side of the coal pillars, considering the water accumulation in the adjacent gob. Material mechanical parameters used in the model are presented in Table 1.

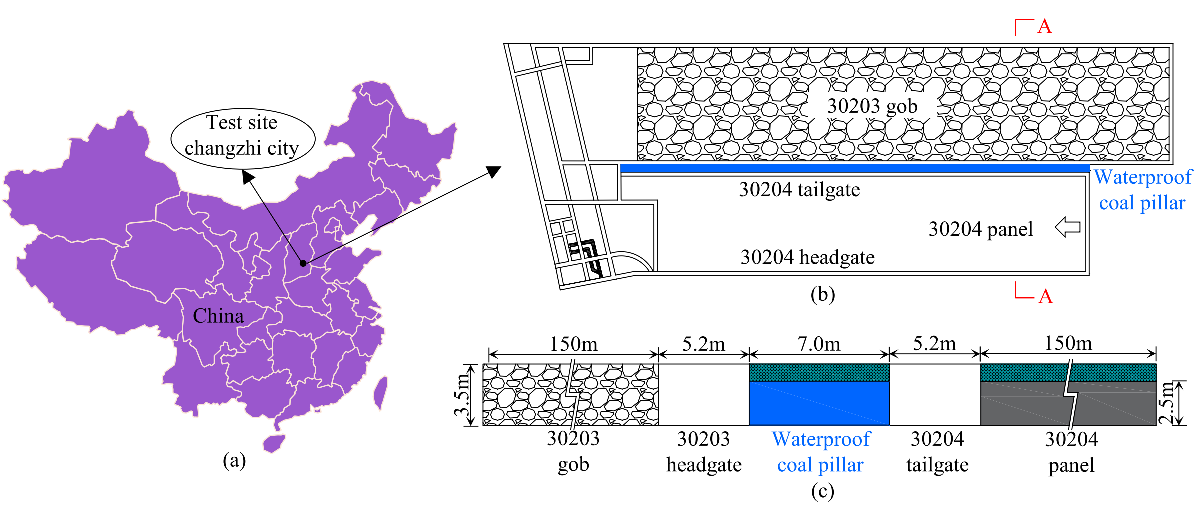

Fig. 8 Layout of working face: **a** mine location; **b** plan view; **c** section A–A

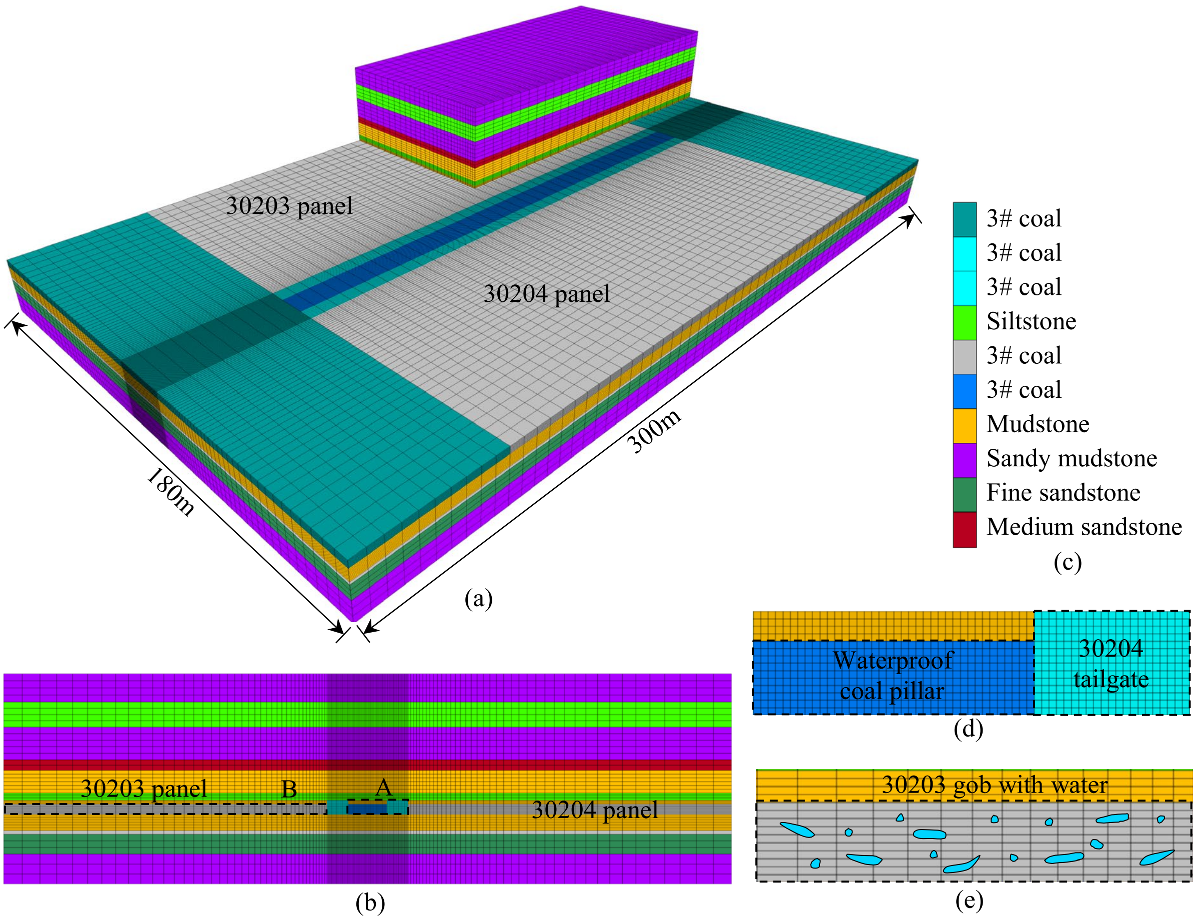

Fig. 10 Numerical calculation model: **a** overall diagram; **b** cross section view; **c** legend; **d** area A; **e** area B

3.3 Mechanical characteristics of gob

The formula for calculating the height of caving zone is as follows (Chen et al. 2023):

$$h_c = \frac{100h_m}{c_1 h_m + c_2} \tag{10}$$

where, h_c is the height of caving zone; h_m is the height of mining; c_1 and c_2 are correction factors, and their values can be found in Table 2.

For the mine with a mining height of 2.5 m and average roof rock strength greater than 20 MPa and less than 40 MPa, the appropriate parameters from Table 2 are chosen and plugged into the formula to calculate the caving zone height, which results in 8.1 m.

The Salamon theoretical model is used to describe the stress–strain relationship of the gob rock mass (Salamon and Munro 1967, Salamon and Ozbay 1998). The formula is given as:

$$\sigma = \frac{E_0 \varepsilon_g}{1 - \varepsilon_g / \varepsilon_{gmax}} \tag{11}$$

where, σ is the vertical stress acting on the gob rock mass; ε_g is the strain that occurs in the gob rock mass under the influence of vertical stress; E_0 is the initial modulus of the gob material, which can be calculated using the following formula:

$$\varepsilon_{gmax} = \frac{b_g - 1}{b_g} \tag{12}$$

Table 1 Mechanical parameters of the model

Lithology	Thickness/m	Density/(kg/m^3)	Bulk modulus/GPa	Shear modulus/GPa	Cohesion/MPa	Friction angle/(°)	Tensile strength/MPa
Sandy mudstone	7.0	2280	3.15	1.97	2.04	31	0.65
Siltstone	6.2	2420	4.89	3.36	2.55	33	1.03
Sandy mudstone	8.1	2280	3.15	1.97	2.04	31	0.65
Medium sandstone	2.6	2610	9.52	6.85	4.17	35	2.96
Mudstone	5.6	2250	2.88	1.73	1.65	30	0.60
Siltstone	1.8	2420	4.89	3.36	2.55	33	1.03
Mudstone	1.0	2250	2.88	1.73	1.65	30	0.60
3# Coal	2.5	1350	1.63	0.84	1.12	29	0.33
Mudstone	4.0	2250	2.88	1.73	1.65	30	0.60
Coal	0.9	1350	1.63	0.84	1.12	29	0.33
Fine sandstone	4.9	2660	9.85	7.33	4.52	36	3.15
Sandy mudstone	7.4	2280	3.15	1.97	2.04	31	0.65

Table 2 Calculation coefficients for average caving zone height (Chen et al. 2024b)

Strata lithology	Compressive strength	Coefficients	
		c_1	c_2
Strong and hard	> 40	2.1	16
Medium strong	20–40	4.7	19
Soft and weak	< 20	6.2	32

where, b_g is the crushing expansion coefficient of the gob material; ε_{gmax} maximum strain of rock mass in gob.

$$b_g = \frac{h_c + h_m}{h_c} \tag{13}$$

$$E_0 = \frac{10.39\sigma_c^{1.042}}{b_g^{7.7}} \tag{14}$$

where σ_c is the strength of rock mass in the caving zone.

Based on laboratory tests, the average uniaxial compressive strength of the roof rock layer is 35 MPa. Plugging this value into the above formula, the dilation coefficient of the gob material is calculated as 1.3086, the maximum strain is 0.2358, and the initial modulus is 53.2257 GPa. The stress–strain relationship of the gob rock mass is shown in Table 3.

Table 3 Stress–strain relationship of the gob rock mass

Strain	Stress/MPa	Strain	Stress/MPa
0.01	0.56	0.12	13.01
0.02	1.16	0.13	15.42
0.03	1.83	0.14	18.34
0.04	2.56	0.15	21.94
0.05	3.38	0.16	26.49
0.06	4.28	0.17	32.43
0.07	5.30	0.18	40.49
0.08	6.44	0.19	52.07
0.09	7.75	0.20	70.12
0.10	9.24	0.21	102.16
0.11	10.97	0.22	174.76

After the mining of the coal, the rock mass in the gob undergoes a process of collapse followed by gradual compaction, experiencing continuous changes in stress and deformation. The double-yield model can more accurately describe the nonlinear behavior of rock mass and the stress recovery process (Chen et al. 2024a). In this study, a single element block with a side length of 1m is used to conduct uniaxial compression tests in FLAC^{3D}. The model was constrained at the bottom and around its perimeter to prevent displacement, while a vertical load of 10^{-5} m/step was applied at the top to mimic the actual loading conditions. The simulated results are compared with the data from Table 3, and the

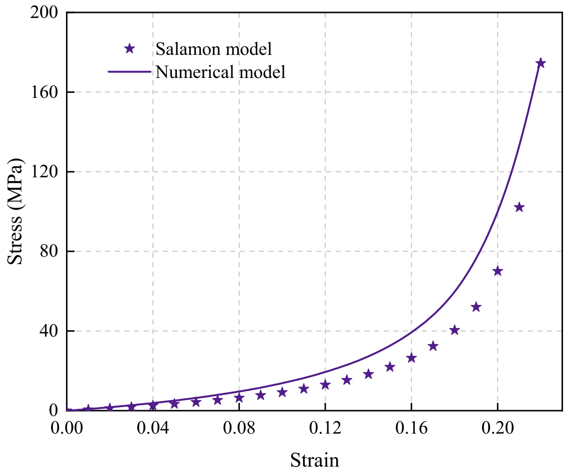

Fig. 11 stress–strain relationship of gob material

Table 4 Materials parameters of gob

Property	Density/ (kg/m^3)	Bulk modulus/GPa	Shear modulus/GPa	Friction angle/ (°)	Dilation angle (°)
Value	1650	7.2	4.4	20	9

comparative analysis is presented in Fig. 11. Based on this comparison, the material parameters for the gob are determined and listed in Table 4.

3.4 Verification of stress environment

To ensure the accuracy of the numerical simulation results, double-yield model is applied to 30,203 gob and overlying collapsed zone rock mass, followed by an equilibrium run. To validate the stress environment, a measurement line was arranged along the strike of working face. As depicted in Fig. 12, at a distance of 80 m from the edge of 30,203 gob, vertical stress has recovered to 99% of virgin stress, reaching 7.62 MPa. On the solid coal side, the stress reaches its peak value of 24.0 MPa at a distance of 8 m from the roadway surface.

3.5 Verification of coal pillar immersion environment

After the stable mining of 30,203 panel, 30,203 gob starts accumulating water. A water pressure of 0.1 MPa was applied to the side edge of the coal pillar near the gob to simulate the erosive effect of accumulated water in the gob on the coal pillar. Following the fluid–structure interaction system described in Chapter 2, perform 50 cycles of calculation, with each cycle consisting of 1000 steps. Five monitoring points are strategically placed inside the coal pillar to observe the variation of pore pressure at different locations, as illustrated in Fig. 13.

The results of water pressure monitoring at points A-E are shown in Fig. 14. After 50 cycles of operation, the water pressure at each measuring

Fig. 12 Stress distribution in numerical simulation

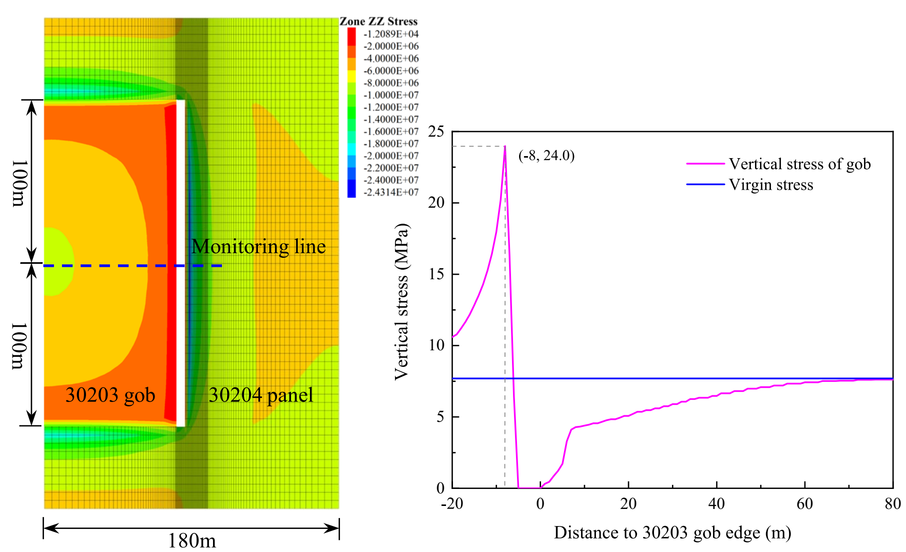

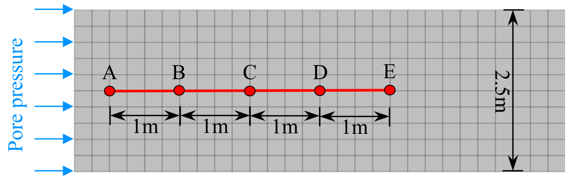

Fig. 13 Layout of measuring points

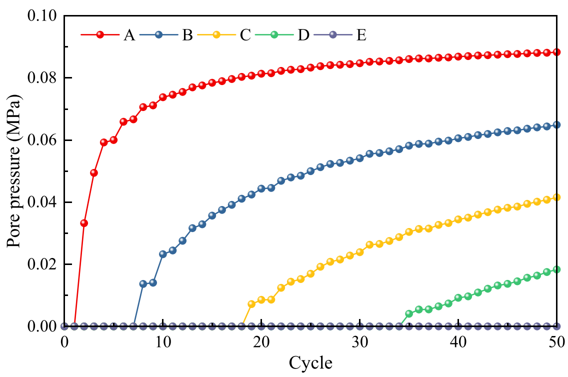

Fig. 14 Pore pressure of coal pillar under different iteration times

point tended to stabilize, indicating that the water seepage inside the coal pillar had stabilized. At Point A, the water pressure reaches 0.09 MPa, which is close to the 0.1 MPa applied at the surface of roadway. Moving from the waterproof coal pillar surface towards its interior, the water pressure gradually decreases, and at Point E, the water pressure remains at 0 MPa. This indicates that during this period, no water infiltration occurs at Point E.

4 Stability of waterproof coal pillar under fluid–structure interaction

4.1 Development of vertical stress in waterproof coal pillar

The left side of waterproof coal pillar is adjacent to 30,203 gob, while the right side is adjacent to 30,204 tailgate. Based on the three stages defined according to the actual mining conditions, vertical stress distribution within waterproof coal pillar at each stage is depicted in Fig. 15.

(1) *Stage 1* Under the influence of the mining of 30,203 panel, waterproof coal pillar reaches its peak stress of 25.6 MPa at a distance of 2.25 m from the surface of 30,203 tailgate.
(2) *Stage 2* The left side of waterproof coal pillar is affected by the softening effect of water intrusion, leading to a reduction in its load-carrying capacity. As a result, the stress peak diminishes to 22.1 MPa, representing a decrease of 13.7%. Due to the degradation of mechanical properties in the water-inundated area on the left side, stress is transferred predominantly towards the right side.
(3) *Stage 3* Waterproof coal pillar is affected by the excavation of 30,204 tailgate. The stress peak experiences a slight increase to 26.2 MPa and shifts towards the right side by 0.75 m.

4.2 Water-barrier performance of waterproof coal pillar

Using the FLAC^{3D} fluid–structure interaction system developed in Fig. 7, permeability and water-softening coefficient are dynamically updated, and the

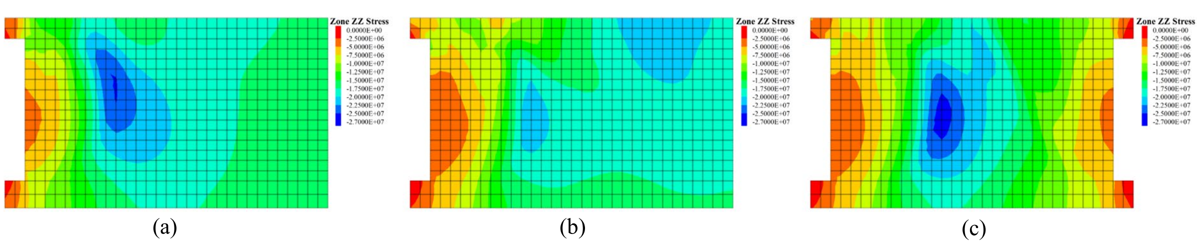

Fig. 15 Vertical stress distribution at different stages of waterproof coal pillar: **a** stage 1; **b** stage 2; **c** stage 3

combination of deviatoric stress, plastic zone, and seepage zone for three stages is obtained, as illustrated in Fig. 16.

(1) *Stage 1* During this stage, waterproof coal pillar is only influenced by the mining activities of 30,203 panel, and the width of plastic zones reaches 2.25 m. Points a–d are all in elastic state.
(2) *Stage 2* The left side of waterproof coal pillar is affected by water infiltration, causing plastic zones to expand into deeper parts of coal pillar. Point a is located in seepage zone, and although plastic failure has not occurred yet, its load-carrying capacity has been reduced, with the deviatoric stress at point a decreasing from 7.0 to 6.5 MPa.
(3) *Stage 3* The waterproof coal pillar is affected by the excavation of 30,204 tailgate, resulting in the extension of both plastic zone and seepage zone towards the interior of coal pillar. At this stage: point a transition from elastic state to plastic state; point b enters seepage zone; point c remains water-free and in elastic state; point d is water-free but in plastic state, indicating a relatively poor water-barrier effect.

In the middle section of waterproof coal pillar, there is a complete region with a width of at least 0.85 m, which remains in elastic state, and the coal remains water-free, with the deviatoric stress ranging from approximately 4–5 MPa. This region exhibits good water-barrier and load-carrying capabilities (Fig. 17).

The waterproof coal pillar undergoes three stages: "mining of 30,203 panel—water infiltration and softening—excavation of 30,204 tailgate". The damage degree of waterproof coal pillar in each stage is as follows:

Stage 1: The damage degree is 25.3%.
Stage 2 The damage degree is 31.4%.
Stage 3 The damage degree is 64.6%.

These damage values represent the extent to which the waterproof coal pillar has been affected and weakened during each stage of the mining process. As the mining progresses and water infiltration occurs, the damage to the coal pillar increases, indicating a gradual reduction in its load-carrying capacity and stability.

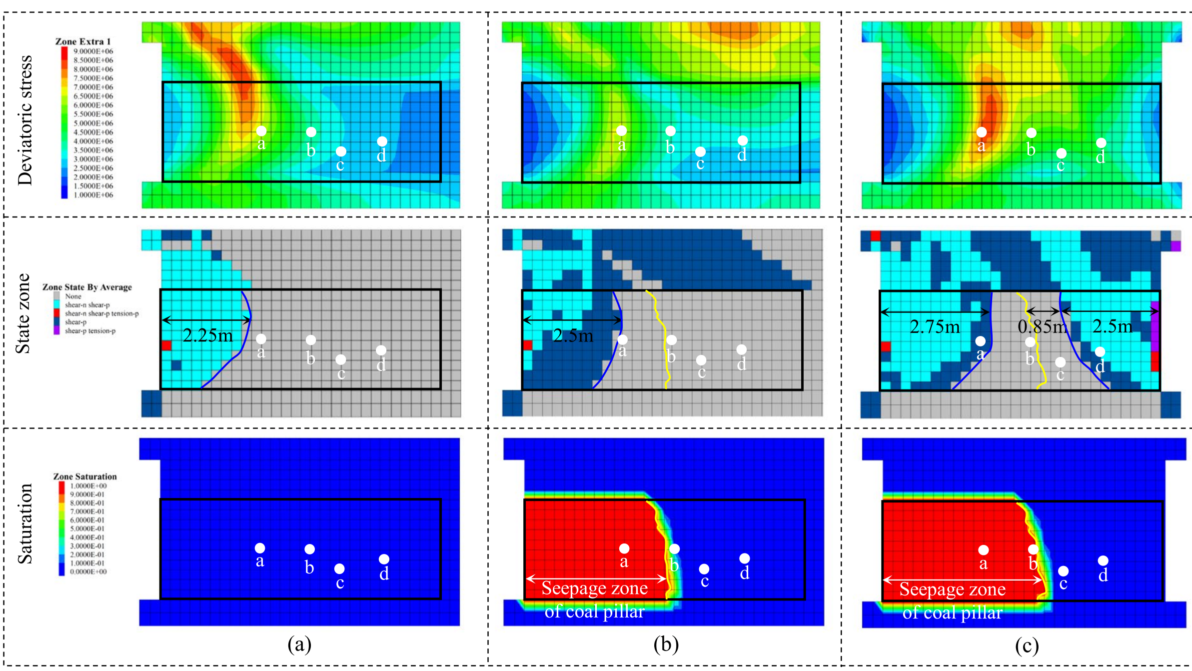

Fig. 16 Water blocking performance of waterproof coal pillar under fluid–structure interaction: **a** stage 1; **b** stage 2; **c** stage 3

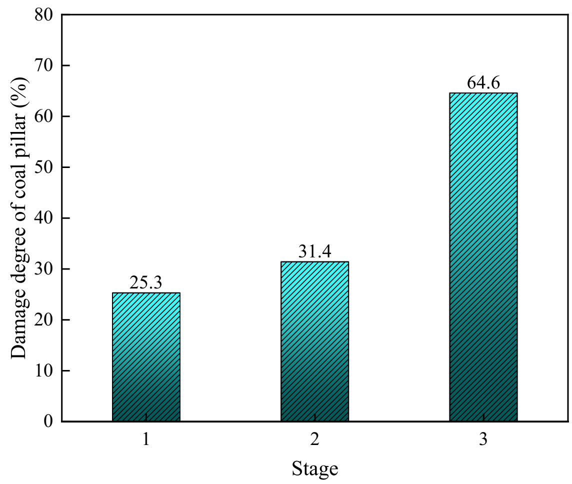

Fig. 17 Damage degree of coal pillar

4.3 Stability analysis of different width waterproof coal pillars

The comparative stability analysis of five different width waterproof coal pillars (3 m, 5 m, 7 m, 9 m, 11 m) is presented in Fig. 18.

For the 3 m width pillar, plastic zones of coal pillar are completely connected, and there is no concentration of vertical stress within it. The overall induced stress is relatively low, resulting in a loss of load-bearing capacity for coal pillar.

For the 5 m width pillar, noticeable stress concentration occurs at the center of coal pillar, indicating that it possesses some load-bearing capacity. However, plastic zones inside coal pillar are interconnected, rendering it ineffective in providing adequate water isolation.

For the 7 m width pillar, the induced deviatoric stress peak zone exhibits a crescent-shaped distribution near the gob side of coal pillar. Plastic zones inside coal pillar is not fully interconnected, with a 1.75 m undamaged section.

For the 9 m width pillar, the vertical stress shifts towards the right side, leading to a larger range of deviatoric stress peak zone near 30,204 tailgate side of coal pillar. Plastic zones on the right side is significantly deeper than that on the left side. Compared to the 7 m width pillar, the undamaged zone width increases by only 0.25 m, indicating that the 9 m width pillar poses greater challenges to the surrounding roadway support.

For the 11 m width pillar, plastic zones on both sides of coal pillar exhibit an approximately symmetric distribution. The depth of plastic zones on the right side decreases significantly, and the width of undamaged zone in the middle reaches 6.0 m. The deviatoric stress peak zone on the left side of coal pillar changes from a wide crescent shape to a narrow one, while the deviatoric stress peak zone on the right side shifts upwards and is predominantly located within the overlying mudstone.

The internal stress-damage conditions of the different width waterproof coal pillars are depicted in Fig. 19.

For the 3 m width pillar, the stress peak is only 7.7 MPa, indicating poor load-bearing capacity, and the damage level reaches 100%. As the width of coal pillar increases from 5 to 11 m, the stress curve gradually transforms from a single-peak shape to a double-peak shape, and the stress peak shifts towards the right side. Consequently, the damage level of coal pillar decreases from 94.5% at 5 m width to 40.5% at 11 m width.

5 Conclusion

This study utilized numerical simulations to investigate the failure characteristics and optimal width of waterproof coal pillars along the gob-side roadway under the influence of mining, excavation and seepage coupling. The main conclusions are as follows:

(1) A numerical model for fluid–structure interaction of waterproof coal pillar was established, and a Fish language program was developed to account for the weakening of coal due to water immersion. This method enables the dynamic coupling of permeability parameters and coal pillar mechanical properties by calculating the weakening coefficient of elastic modulus, cohesion, and friction angle based on its water saturation.

(2) The coupling characteristics of stress distribution, plastic zone, and seepage zone of waterproof coal pillars were revealed during the "mining—water immersion softening—roadway excavation" stages. The region where both seepage and plasticity coexist is the primary area responsible for water drainage in waterproof coal pillar. The area where seepage occurs but remains elastic repre-

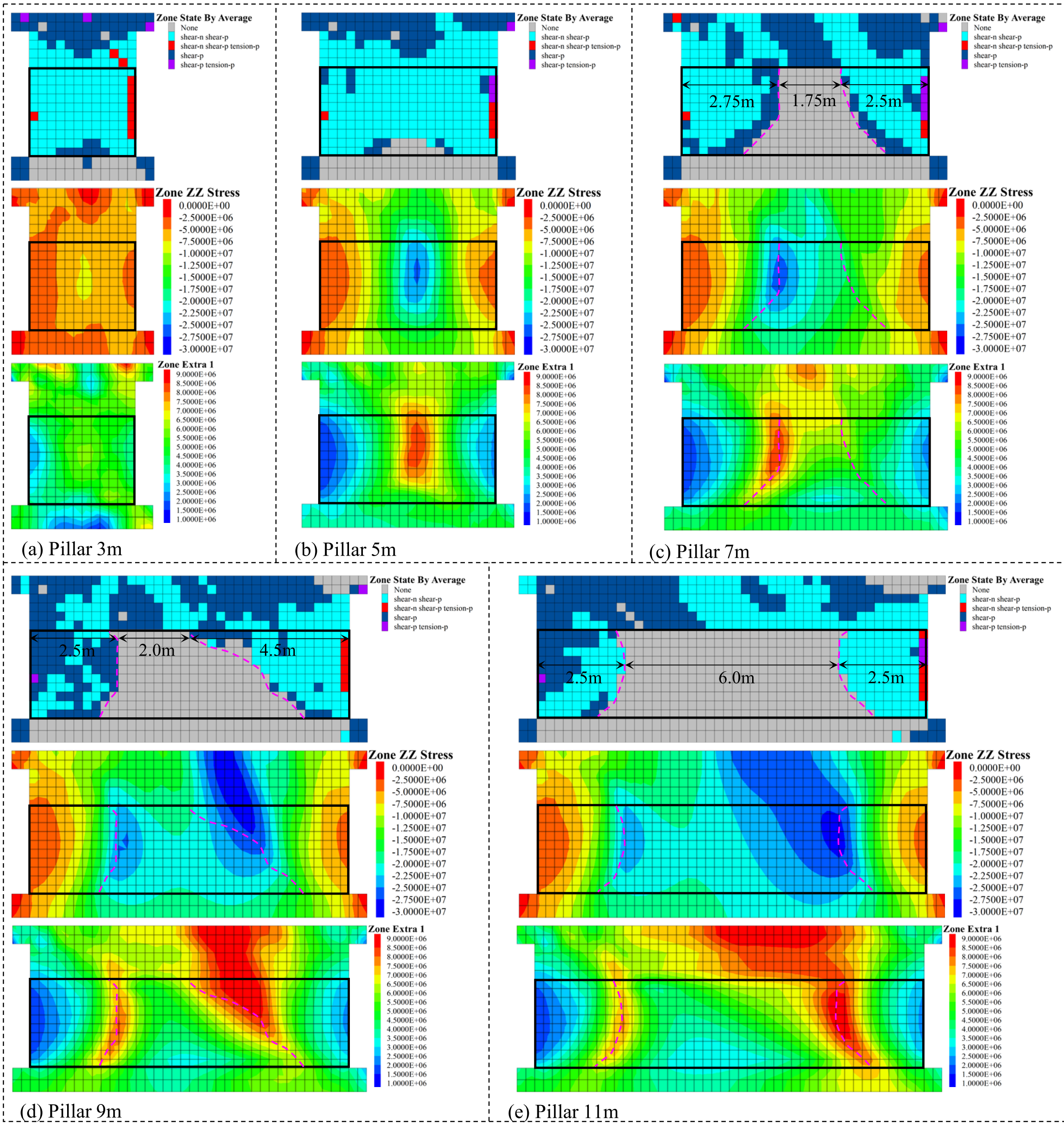

Fig. 18 Stability of waterproof coal pillars with different widths

sents the maximum diffusion boundary of water drainage, while the area without seepage but with elasticity plays a vital role in determining the water resistance of coal pillar.

(3) The water resistance capacity of waterproof coal pillars depends on the extent of the seepage area on the gob side and the plastic zones on both sides. Under the conditions of 30,204 panel, when the width of waterproof coal pillar is 3 m and 5 m, plastic zones are interconnected, forming water drainage channels. Conversely, for widths of 7 m, 9 m, and 11 m, seepage zones and plastic zones are not connected, indicating that

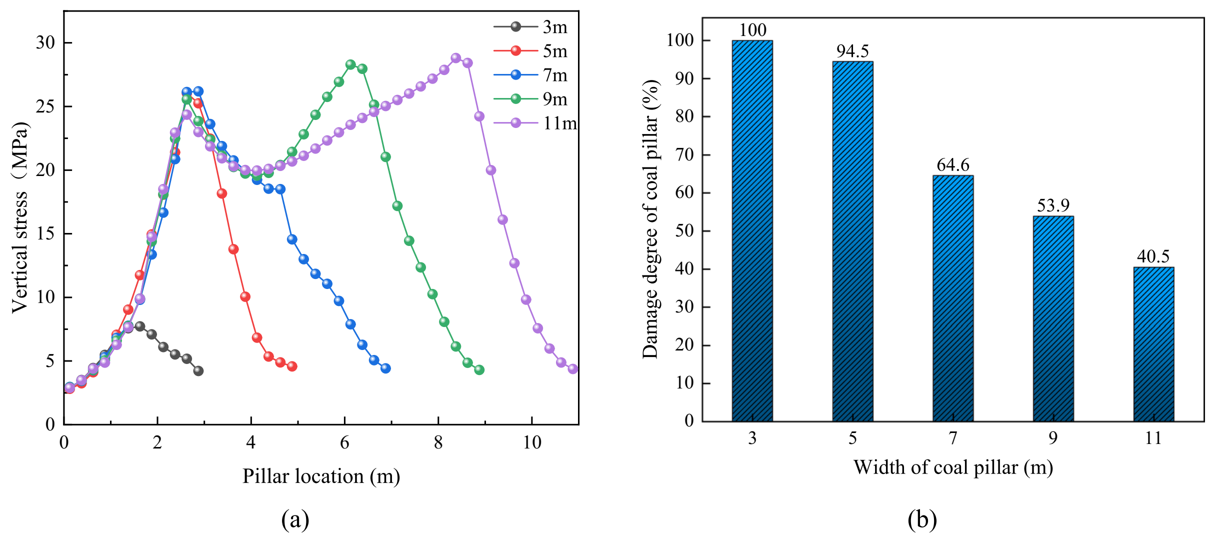

Fig. 19 Internal stress-damage situation of waterproof coal pillar: **a** vertical stress; **b** damage degree

coal pillar possesses load-bearing and water-isolating characteristics.

Future research endeavors could leverage advanced sensing devices and techniques for field investigations to validate the results obtained from numerical simulations. Conducting on-site studies will provide real data to corroborate the accuracy of our model and further enhance its predictive capabilities.

Author contributions Xiangyu Wang presented the idea, Dingchao Chen wrote the main manuscript text, Jianbiao Bai and Menglong Li wrote the theoretical analysis and numerical simulations, all authors reviewed the manuscript. All authors read and approved the final manuscript.

Funding This research was financially supported by Graduate Innovation Program of China University of Mining and Technology (2024WLKXJ018), Postgraduate Research & Practice Innovation Program of Jiangsu Province (KYCX24_2852), National Key Research and Development Program of China (2023YFC2907600), Independent research project of State Key Laboratory of Coal Resources and Safe Mining, CUMT (SKLCRSM22X007).

Data availability Data will be made available on request.

Declarations

Ethical approval Not applicable.

Consent for publication The authors have approved and consented to publish the manuscript.

Conflict of interest The authors declared that there is no conflict of interest.

References

Bukowski P (2015) Evaluation of water hazard in hard coal mines in changing conditions of functioning of mining industry in upper Silesian coal basin—USCB (Poland). Arch Min Sci 60:455–475

Chen L, Feng X, Xie W, Zeng W, Zheng Z (2017) Using a fluid-solid coupled numerical simulation to determine a suitable size for barrier pillars when mining shallow coal seams beneath an unconsolidated, confined aquifer. Mine Water Environ 36:67–77

Chen D, Wang X, Zhang F, Li M, Zhao X, Li G, Yu Y, Wang G, Zhao J, Wang X (2022a) Research on directional controllability of cracking in hydraulic fracturing of hard overburden based on local stress field intervention. Energies 15:4252

Chen L, Zhang D, Yao N, Wang L, Fan G, Wang X, Zhang W (2022b) Coupling influence of inclination angle and moisture content on mechanical properties and microcrack fracture of coal specimens. Lithosphere 2021:6226445

Chen D, Wang X, Wu S, Zhang F, Fan Z, Wang X, Li M (2023) Study on stability mechanism and control techniques of surrounding rock in gob-side entry retaining with flexible formwork concrete wall. J Central South Univ 30:2966–2982

Chen D, Wang X, Bai J, Li M, Lu J, Zhang F, Sun S, Zhao X, Yu Y (2024a) The full cycle evolution law of energy-stress in the surrounding rock of the gob-side entry driving for adjacent advancing working face. Coal Sci Technol 1–14

Chen D, Wang X, Zhang F, Bai J, Zhao X, Li M, Yu Y, Wang X, Sun S (2024b) Study on the mechanism of progressive instability of special-shaped coal pillar and the stability control of roadway under the influence of mining. Rock Mech Rock Eng

Cui F, Wu Q, Lin Y, Zeng Y, Zhang K (2018) Damage features and formation mechanism of the strong water inrush disaster at the daxing Co mine, Guangdong Province, China. Mine Water Environ 37:346–350

Dash AK, Bhattacharjee RM, Paul PS (2016) Lessons learnt from Indian inundation disasters: an analysis of case studies. Int J Disaster Risk Reduct 20:93–102

Fang Z, Liu L, Zhang X, Han K, Wang J, Zhu M, Sun W, He W, Gao Y (2023) Carbonation curing of modified magnesium-coal based solid waste backfill material for CO_2 sequestration. Process Saf Environ Prot 180:778–788

Fangpeng C, Qiang W, Shuai Z, Ningan W, Yuan J (2018) Damage characteristics and mechanism of a strong water inrush disaster at the Wangjialing coal mine, Shanxi Province, China. Geofluids 2018:3253641

Galav A, Singh GSP, Sharma SK (2022) A numerical modeling approach for assessment of seepage characteristics and performance of protective water barrier pillars in underground coal mines. Min Metall Explor 39:2047–2063

Gui H, Lin M (2016) Types of water hazards in China coalmines and regional characteristics. Nat Hazards 84:1501–1512

Han P, Zhang C, Wang W (2022) Failure analysis of coal pillars and gateroads in longwall faces under the mining-water invasion coupling effect. Eng Fail Anal 131:105912

He Y, Huang Q (2022) Research on roof structure and determination of working resistance of shallow buried single key stratum based on grid drillhole field method. Lithosphere 2021:4328618

He Y, Huang Q, Wei Y, Du J (2023) Research on roof load transfer by passing coal pillar of working face in shallow buried closely multiple-seam. Minerals 13

Hu M, Zhao W, Lu Z, Ren J, Miao Y (2019) Research on the reasonable width of the waterproof coal pillar during the mining of a shallow coal seam located close to a reservoir. Adv Civ Eng 2019:3532784

Li A, Ji B, Ma Q, Liu C, Wang F, Ma L, Mu P, Mou L, Yang Y, Ding X (2021) Design of longwall coal pillar for the prevention of water inrush from the seam floor with through fault. Geofluids 2021:5536235

Li Z, Fan J, Feng G, Zhang H, Qi C, Zhang J (2023) Failure characteristics and reasonable width of water resisting pillar under the coupling effect of mining and seepage. J China Coal Soc 1–14

Liu S, Wang W, Wang Q, Jiang J, Li H, Peng H (2020) Study on stability of coal pillars of roadway excavated along gob with water in gently inclined coal seam. Coal Sci Technol 48:78–87

Liu Q, Xue Y, Ma D, Li Q (2023a) Failure characteristics of the water-resisting coal pillar under stress-seepage coupling and determination of reasonable coal pillar width. Water

Liu S, Fei Y, Wang J, Wu D, Guo D, Dong Y, Liu X, Shangguan Y (2023b) A novel method to retain a waterproof coal pillar near water-conducting fault. J Geophys Eng 20:225–239

Lu Y, Zhou Z, Ge Z, Zhang X, Li Q (2016) Coupling effect of intruding water and inherent gas on coal strength based on the improved (Mohr-Coulomb) failure criterion. Minerals

Ma D, Bai H (2015) Groundwater inflow prediction model of karst collapse pillar: a case study for mining-induced groundwater inrush risk. Nat Hazards 76:1319–1334

Ma D, Wang J, Li Z (2019) Effect of particle erosion on mining-induced water inrush hazard of karst collapse pillar. Environ Sci Pollut Res 26:19719–19728

Ma D, Duan H, Cai X, Li Z, Li Q, Zhang Q (2018) A global optimization-based method for the prediction of water inrush hazard from mining floor. Water

Ma D, Duan H, Zhang J, Bai H (2022) A state-of-the-art review on rock seepage mechanism of water inrush disaster in coal mines. Int J Coal SciTechnol 9:50

Maiti J, Khanzode VV, Ray PK (2009) Severity analysis of Indian coal mine accidents—a retrospective study for 100 years. Saf Sci 47:1033–1042

Polak K, Różkowski K, Czaja P (2016) Causes and effects of uncontrolled water inrush into a decommissioned mine shaft. Mine Water Environ 35:128–135

Salamon MDG, Munro A (1967) A study of the strength of coal pillars. J South Afr Inst Min Metall 68

Salamon MDG, Ozbay MU (1998) Life and design of bord-and-pillar workings affected by pillar scaling. J South Afr Inst Min Metall 98:135–145

Shan R, Li Z, Wang C, Wei Y, Bai Y, Zhao Y, Tong X (2021) Research on the mechanism of asymmetric deformation and stability control of near-fault roadway under the influence of mining. Eng Fail Anal 127:105492

Shao J, Zhang W, Wu X, Lei Y, Wu X (2022) rock damage model coupled stress-seepage and its application in water inrush from faults in coal mines. ACS Omega 7:13604–13614

Singh KKK (2015) MineVue radar for delineation of coal barrier thickness in underground coal mines: case studies. J Geol Soc India 85:247–253

Sun W, Zhou W, Jiao J (2016) Hydrogeological classification and water inrush accidents in China's coal mines. Mine Water Environ 35:214–220

Wang H (2006) Fluid-solid coupling analysis of the safety of the waterproof coal pillar. M.S. Shandong University, People's Republic of China

Wang W, Wang H, Li D, Li H, Liu Z (2018) Strength and failure characteristics of natural and water-saturated coal specimens under static and dynamic loads. Shock Vib 2018:3526121

Wang R, Bai J, Yan S, Pan G, Zhang D, Zhu Q (2021) Structure partition and reasonable width determination of waterproof coal pillar in strip mining. Lithosphere 2021:3339797

Wang D, Sui W, Ranville JF (2022a) Hazard identification and risk assessment of groundwater inrush from a coal mine: a review. Bull Eng Geol Environ 81:421

Wang YQ, Wang X, Zhang JS, Yang BS, Zhu WJ, Wang ZP (2022b) Similar experimental study on retaining waterproof coal pillar in composite strata mining. Sci Rep 12:1366

Wang Z, Zhang J, Li J, Wang P, Wu C, Shi L (2022c) Research of surrounding rock control of gob-side entry retaining based on deviatoric stress distribution characteristics. Sustainability

Xue Y (2017) Study on the permeability evolution offractured coal under the influence of mining. China University of Mining and Technology

Yao Q, Tang C, Xia Z, Liu X, Zhu L, Chong Z, Hui X (2020) Mechanisms of failure in coal samples from underground water reservoir. Eng Geol 267:105494

Yao Q, Wang W, Li X, Tang C, Xu Q, Yu L (2021a) Study of mechanical properties and acoustic emissioncharacteristics of coal measures under water-rock interaction. J China Univ Min Technol 50:558–569

Yao Q, Yu L, Chen N, Wang W, Xu Q (2021b) Experimental study on damage and failure of coal-pillar dams in coal mine underground reservoir under dynamic load. Geofluids 2021:5623650

Yao Q, Yan H, Li X, Yao W, Wang F (2022) The construction and application of a coupled parameter transfer system for fluid-mechanical model. J Min Saf Eng 39:429–440

Yin S, Wang Y, Li W (2023) Cause, countermeasures and solutions of water hazards in coal mines in China. Coal Geol Explor 51:214–221

Zhang M, Nie R (2020) Experimental Investigation on the influence of water content on the mechanical properties of coal under conventional triaxial compression. Shock Vib 2020:8872438

Zhang C, Liu J, Zhao Y, Zhang L, Guo J (2019a) A fluid-solid coupling method for the simulation of gas transport in porous coal and rock media. Energy Sci Eng 7:1913–1924

Zhang T, Gan Q, Zhao Y, Zhu G, Nie X, Yang K, Li J (2019b) Investigations into mining-induced stress–fracture–seepage field coupling effect considering the response of key stratum and composite aquifer. Rock Mech Rock Eng 52:4017–4031

Zhang C, Han P, Wang F, He X (2021) The stability of residual coal pillar in underground reservoir with the effect of mining and water immersion. J China Univ Min Technol 50:220–227

Zhang C, Bai Q, Han P (2023) A review of water rock interaction in underground coal mining: problems and analysis. Bull Eng Geol Env 82:157

Zhao Y, Liao J, Liu Q, Li Y, Cheng J (2020) Linkage analysis between solid-fluid coupling and the strength reduction method for karst cave water inrush in mines. Shock Vib 2020:5415812